Design, Synthesis, *In-Silico* Study of Novel Benzofuran Thiazolyl Hydrazones as Anticancer Agents Targeting EGFR Kinase

Sonali Sandeep Shinde[1], Jaydeo Tirthraj Kilbile[2], Sachin Shivling Bhusari[1], and Pravin Shridhar Wakte[1*]

[1]*Department of Chemical Technology, Dr. Babasaheb Ambedkar Marathwada University, Chhatrapati Sambhajinagar, 431004 Maharashtra, India*

[2]*Department of Chemistry, School of Basic and Applied Sciences, MGM University, Chhatrapati Sambhajinagar, 431003 Maharashtra, India*

* ***Corresponding author:***

email: pswakte21@gmail.com

Received: April 18, 2025
Accepted: May 10, 2025

DOI: 10.22146/ijc.106097

Abstract: *In the current investigation, a series of new benzofuran-thiazolyl hydrazones* ***5(a–h)*** *were synthesized, characterized, and tested for anticancer activity against selected cancer cell lines, including A549, MCF-7, and DU-145, using MTT and EGFR enzymatic assays. The synthesized compounds* ***5g*** *and* ***5h*** *showed considerable anticancer activity, with* IC_{50} *values ranging from 9.05 to 18.09 μM and 12.03 to 13.09 μM, respectively. Doxorubicin and osimertinib were used as the standard drugs for comparison of activity. Compounds* ***5g*** *and* ***5h*** *also showed significant antioxidant activity as measured by the DPPH method. The molecular docking investigation was conducted against the EGFR (PDB: 1M17) to learn about the interactions of synthesized compounds with binding pockets. Furthermore, an ADME research and molecular dynamics simulation study was conducted to provide insight into drug-likeness and conformational stability. The results show a good match between reported anticancer effects and computational analyses. Compounds* ***5g*** *and* ***5h*** *exhibited significant cytotoxicity against lung, breast, and prostate cancer cell lines. These findings underscore the potential of benzofuran-thiazolyl hydrazone derivatives as promising candidates for the development of novel anticancer therapeutics.*

Keywords: *benzofuran; thiazole; hydrazone; anticancer; EGFR; molecular docking; enzymatic assay*

■ INTRODUCTION

Cancer is a severe worldwide health hazard, affecting around 19–20 million individuals every year. By 2030, the number of new cancer instances and mortality is anticipated to increase to 24.2 million and 13.1 million, respectively [1]. Cancer is described as abnormal cell growth and proliferation that results in significant physiological abnormalities [2]. Protein kinases are important signal transduction intermediaries that regulate many biological processes, including cell growth, division, migrations, metabolism, and controlled cell death. These tyrosine kinases use ATP to generate the phosphorylation of certain amino acid residues in target proteins, specifically threonine, tyrosine, and serine. Such modifications are necessary for successful communication between cells and maintaining homeostasis [3]. Among protein kinases, tyrosine kinases (TKs) are crucial since their activity is carefully controlled in normal cells. Mutations or structural changes in tyrosine kinases have been linked to the formation and progression of many human cancers. As a result, TKs and their growth-factor ligands were discovered as potential candidates for medical therapy using small-molecule medications [4]. Several tiny molecules of epidermal growth factor receptor (EGFR) inhibitors, either alone or in combination with other licensed anticancer drugs, have been discovered to treat

various types of cancer. These drugs include dasatinib, dabrafenib, gefitinib, osimertinib, and erlotinib [5-8]. According to various research reports, erlotinib and gefitinib were the first EGFR inhibitors [9]. In addition, *N*-heterocyclic derivatives such as triazole [10-11], quinoline [12-13], quinazoline [14-15], pyrimidine [16-17], and thiazole [18-19] were revealed to have EGFR inhibitory activity, making it an ideal strategy for developing novel EGFR inhibitors.

Benzofuran molecules have several uses in drug discovery. They show antibacterial [20], anti-allergic, antioxidant [21], and antitumor [22] effects. Furthermore, benzofuran derivatives show promise as protein kinase blockers [23]. El-Khouly et al. [22] synthesized benzofuran thiazolyl hydrazone I, II, III, and IV (Fig. 1), which had anticancer action by blocking EGFR action. Previous research has demonstrated that benzofuran analogs such as ebenfuran III, iophirone D, and iophirone E are naturally occurring compounds that exhibit anticancer action by blocking EGFR [24]. The thiazole moiety is a frequently used heterocycle in drug development because of its many biological properties [25-26]. Various thiazole compounds have been designed to target specific cellular pathways, and their antiproliferative activities differ correspondingly [27]. Dasatinib and dabrafenib containing a thiazole ring are EGFR inhibitors that have been authorized as cancer treatments. Hydrazones are a prominent structural group found in a range of biologically active compounds [28]. Their diverse antiproliferative effect implies that additional studies should be done on these intriguing molecular structures to discover new promising chemotherapy drugs [29]. These chemical compounds are vital since they may serve as prototypes for supplying critical structural frameworks that may aid medication development in key phases in this quest for effective prospective and innovative derivatives.

Despite substantial advances in cancer treatment, numerous restrictions remain. These include issues with cancer cell selectivity, undesired side effects, and development of resistance to multiple drugs in tumor cells, which renders them unresponsive to existing therapy options [30-31]. As a result, developing innovative tiny molecules that have excellent potency

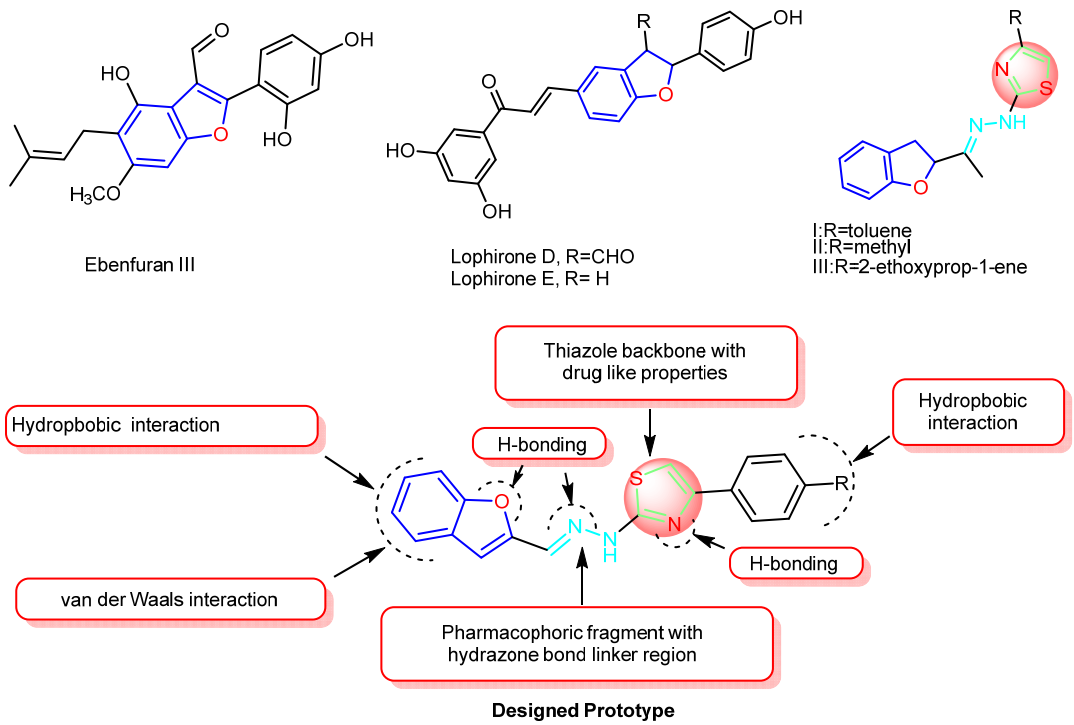

Fig 1. Structures of various recorded benzofuran hybrids and EGFR blockers, using color map molecular hybridization for a rational design

and specificity remains a tough challenge in medical chemistry. Furthermore, the creation of drugs that may overcome resistance to multiple drugs in tumor cells is a critical field of research. Identifying the mechanisms that cause drug resistance and prospective targets or pathways that may be changed to restore drug sensitivity are essential phases of this effort [32]. The investigators can develop and synthesize novel substances that efficiently overcome drug-resistant tumor cells by explaining these processes, using structure-activity relationship findings, computational modeling, and high-throughput screening approaches to determine key substances and optimize their therapeutic effects. In our studies, we developed and synthesized benzofuran thiazolyl hydrazones by linking a modified benzene ring at the thiazole-C_4 position and conjugating the benzofuran structure and thiazole ring via the methylene hydrazinyl linkage at the thiazole-C_2 site (Fig. 1) by considering aspects such as phenyl ring substitutions, which may result in hydrogen bonding with amino acids present in the EGFR's active site, ring size variations, and molecular orientation. The most effective chemical discovered was then studied for enzymatic inhibition and capacity to cause apoptosis, which gave information on its mode of action and promise as an anticancer drug.

■ EXPERIMENTAL SECTION

Materials

All solvents and chemicals used in this study, including benzo[*b*]furan-2-carboxaldehyde (**1**), hydrazine carbothioamide (**2**), substituted bromoacetophenone **5**(**a**–**h**), 3-(4,5-dimethylthiazol-2-yl)-2,5-diphenyltetrazolium bromide (MTT), 1,1-diphenyl-2-picrylhydrazyl (DPPH), fetal bovine serum (FBS), Modified Eagle's Medium (MEM), ethanol, acetic acid, ethyl acetate, and *n*-hexane, were obtained from Avra and TCI laboratory.

Instrumentation

Utilizing thin layer chromatography (TLC) plates that had previously been treated with silica gel 60 F-254 aluminum by Merck, the progression of the reaction was monitored each hour under an ultraviolet (UV) light source. The melting point of each derivative was determined using the Buchi 530 Melting Point Device. The Fourier-transform infrared (FTIR) spectra were created with Bruker FTIR. DMSO-d_6 was used as the solvent to generate the proton and carbon nuclear magnetic resonance (^{1}H-NMR (500 MHz) and ^{13}C-NMR (125 MHz)) spectra on the Bruker Avance-II NMR spectrometer. Tetramethylsilane was employed as an NMR technique standard within the procedure. Chemical shift readings are given in parts per million (ppm), and the coupling constant (*J*) is provided in Hz. The double doublet (*dd*), triplet (*t*), multiple (*m*), singlet (*s*), and broad singlet (*brs*) are the acronyms for the NMR splitting pattern. The micro mass was verified using an electron spin impact (ESI) source that was mounted Q-TOF on a Waters.

Procedure

Synthesis of compounds 5(a–h)

In a dry round bottom flask, compounds **1** (1.0 mol equivalent), and **2** (1.0 mol equivalent) were added in 4–5 mL of ethanol in the presence of 2–3 drops of acetic acid functioning as a catalyst. After 2 h of mixing the reaction ingredients at 75–80 °C, the progression of the reaction was observed on a TLC utilizing a 3:7 ethyl acetate:*n*-hexane mobile system. After completion of the reaction, compound **5**(**a**–**h**) (1.0 mol equivalent) was added and stirred for an additional 4 h at ambient temperature [33]. TLC was used to continuously monitor the progression of the reaction using a 10% chloroform: methanol solvent solution. The solid product **5**(**a**–**h**) was cooled to room temperature to achieve the final pure derivatives, filtered, dried, and recrystallized from ethanol [34]. All spectroscopic data can be found in Fig. S1-S32.

2-(2-(benzofuran-2-ylmethylene)hydrazineyl)-4-(4-nitrophenyl)thiazole (5a). Dark-yellow solid; Yield: 90%; FTIR (KBr, ν cm^{-1}): 3303 (N–H stretch), 1569 (C=N stretch), 1497 and 1323 (–NO_2 stretch), 1276 (C–N stretch thiazole), 1148, 1102 (C–N, C–O stretch), 851 (C–S–C stretch); ^{1}H-NMR (DMSO-d_6, 500 MHz): 12.53 (*bs*, 1H), 8.30–8.27 (*m*, 2H), 8.13–8.11 (*m*, 2H), 8.08 (*s*, 1H), 7.77 (*s*, 1H), 7.69–7.65 (*m*, 2H), 7.39–7.36 (*m*, 1H), 7.30–7.27 (*m*, 2H); ^{13}C-NMR (125 MHz,

DMSO-d_6): 168.06, 154.61, 151.10, 148.56, 146.25, 140.53, 131.67, 127.94, 126.35, 125.79, 124.12, 123.44, 121.63, 111.31, 108.99, 108.86; HRMS Calcd. for $C_{18}H_{12}N_4O_3S$: *m/z* 364.0630, Found 365.0713 $[M+H]^+$.

2-(2-(benzofuran-2-ylmethylene)hydrazineyl)-4-(4-chlorophenyl)thiazole (5b). Light-yellow solid; Yield: 86%; FTIR (KBr, ν cm^{-1}): 3056 (N–H stretch), 1576 (C=N stretch), 1434 (C=C stretch), 1291 (C–N stretch thiazole), 1010, 1093 (C–N, C–O, C–Cl stretch), 836 (C–S–C stretch); ^{1}H-NMR (DMSO-d_6, 500 MHz): 12.54 *(bs*, 1H), 8.06 (*s*, 1H), 7.68–7.61 (*m*, 3H), 7.35–7.28 (*m*, 5H), 7.27–7.23 (*m*, 2H); ^{13}C-NMR (125 MHz, DMSO-d_6): 165.98, 157.69, 154.63, 151.00, 132.80, 129.61, 128.50, 127.92, 125.72, 124.76, 123.39, 122.32, 121.59, 121.53, 111.40, 111.32, 109.12, 104.98; HRMS Calcd. for $C_{18}H_{12}ClN_3OS$: *m/z* 353.039, Found 354.2671 $[M+H]^+$.

2-(2-(benzofuran-2-ylmethylene)hydrazineyl)-4-(*p*-tolyl)thiazole (5c). Cream yellow solid; Yield: 92%; FTIR (KBr, ν cm^{-1}): 3040 (N–H stretch), 1555 (C=N stretch), 1442 (C=C stretch), 1250 (C–N stretch thiazole), 1152, 1092 (C–N, C–O stretch), 827 (C–S–C stretch); ^{1}H-NMR (DMSO-d_6, 500 MHz): 12.50 (*bs*, 1H), 8.05 (*s*, 1H), 7.67–7.57 (*m*, 3H), 7.33–7.27 (*m*, 2H), 7.26–7.21 (*m*, 3H), 7.05 (*d*, *J* = 8.1 Hz, 2H), 2.29 (*s*, 3H); ^{13}C-NMR (125 MHz, DMSO-d_6): 165.72, 158.52, 154.62, 151.11, 137.38, 131.30, 129.01, 127.95, 127.77, 125.65, 124.63, 123.37, 121.56, 111.38, 108.91, 104.60; HRMS Calcd. for $C_{19}H_{15}N_3OS$: *m/z* 333.0936, Found 334.1023 $[M+H]^+$.

4-(2-(2-(benzofuran-2-ylmethylene)hydrazineyl)thiazol-4-yl)phenol (5d). Dark-yellow solid; Yield: 95%; m.p. 227–229 °C; FTIR (KBr, ν cm^{-1}): 3227, 3056 (N–H, O–H stretch), 1622 (C=N stretch), 1283 (C–N stretch thiazole), 1172, 1122 (C–N, C–O stretch), 870 (C–S–C stretch); ^{1}H-NMR (DMSO-d_6, 500 MHz): 11.80 (*s*, 1H), 9.03 (*s*, 1H), 8.28 (*s*, 1H), 7.66–7.63 (*m*, 2H), 7.04 (*s*, 1H), 6.80–6.77 (*m*, 2H), 5.85 (*bs*, 1H), 5.85 (*bs*, 1H), 2.47 (*s*, 3H); ^{13}C-NMR (125 MHz, DMSO-d_6): 168.07, 157.52, 148.07, 143.50, 137.28, 130.24, 129.16, 128.77, 127.24, 124.97, 115.43, 114.51, 101.06; HRMS Calcd. for $C_{18}H_{13}N_3O_2S$: *m/z* 335.0728; Found 336.08 $[M+H]^+$.

2-(2-(benzofuran-2-ylmethylene)hydrazineyl)-4-(4-methoxyphenyl)thiazole (5e). Light-yellow solid; Yield: 87%; FTIR (KBr, ν cm^{-1}): 3061 (N–H stretch), 1607 (C=N stretch), 1494 (C=C stretch), 1315 (C–N stretch thiazole), 1250 (C–O stretch), 1186, 1026 (C–N, C–S stretch); ^{1}H-NMR (DMSO-d_6, 500 MHz): 12.10 (*bs*, 1H), 9.03 (*s*, 1H), 8.28 (*s*, 1H), 7.79–7.76 (*m*, 2H), 7.16 (*s*, 1H), 6.99–6.96 (*m*, 2H), 3.79 (*s*, 3H), 2.48 (*s*, 3H); ^{13}C-NMR (DMSO-d_6, 125 MHz): 167.95, 158.99, 154.29, 151.75, 134.80, 129.67, 128.83, 127.75, 126.98, 114.01, 113.85, 109.02, 55.09, 15.18; HRMS Calcd. for $C_{19}H_{15}N_3O_2S$: *m/z* 349.0885; Found 350.0685 $[M+H]^+$.

4-([1,1'-biphenyl]-4-yl)-2-(2-(benzofuran-2-ylmethylene)hydrazineyl)thiazole (5f). Brown solid; Yield: 85%; FTIR (KBr, ν cm^{-1}): 3150 (N–H stretch), 1558 (C=N stretch), 1444 (C=C stretch), 1255 (C–N stretch thiazole), 1144, 1050 (C–N, C–O stretch), 810 (C–S–C stretch); ^{1}H-NMR (DMSO-d_6, 500 MHz): 12.53 (*bs*, 1H), 8.09–8.08 (*m*, 1H), 7.97–7.95 (*m*, 1H), 7.74–7.71 (*m*, 2H), 7.68–7.65 (*m*, 2H), 7.56–7.53 (*m*, 2H), 7.49–7.44 (*m*, 3H), 7.37–7.24 (*m*, 5H); ^{13}C-NMR (DMSO-d_6, 125 MHz): 167.66, 154.33, 150.93, 139.75, 138.80, 135.27, 129.10, 129.02, 128.92, 127.64, 127.16, 126.82, 126.62, 107.89, 15.27; HRMS Calcd. for $C_{24}H_{17}N_3OS$: *m/z* 395.1092, Found 396.1174 $[M+H]^+$.

4-(2-(2-(benzofuran-2-ylmethylene)hydrazineyl)thiazol-4-yl)benzonitrile (5g). Dark-yellow solid; Yield: 91%; FTIR (KBr, ν cm^{-1}): 3256 (N–H stretch), 2217 (CN stretch), 1567 (C=N stretch), 1422–1569 (C=C stretch)), 1276 (C–N stretch thiazole), 1135, 1045 (C–N, C–O stretch), 839 (C–S–C stretch); ^{1}H-NMR (DMSO-d_6, 500 MHz): 12.53 (*bs*, 1H), 8.30–8.27 (*m*, 2H), 8.13–8.11 (*m*, 2H), 8.08 (*s*, 1H), 7.77 (*s*, 1H), 7.69–7.65 (*m*, 2H), 7.39–7.36 (*m*, 1H), 7.30–7.27 (*m*, 2H); ^{13}C-NMR (125 MHz, DMSO-d_6): 167.95, 154.60, 151.13, 150.90, 138.62, 132.69, 131.57, 127.88, 126.11, 125.75, 123.43, 121.61, 118.95, 111.30, 109.65, 108.76, 107.97; HRMS Calcd. for $C_{19}H_{12}N_4OS$: *m/z* 344.0732, Found 345.0805 $[M+H]^+$.

2-(2-(benzofuran-2-ylmethylene)hydrazineyl)-4-(4-(trifluoromethyl)phenyl)thiazole (5h). Yellow solid; Yield: 95%; FTIR (KBr, ν cm^{-1}): 3066 (N–H stretch), 1612 (C=N stretch), 1490 (C=C stretch), 1322 (C–N stretch thiazole), 1174, 1115, 1069 (C–N, C–S stretch), 948 (C–F stretch); ^{1}H-NMR (DMSO-d_6, 500 MHz):

12.63 (*bs*, 1H), 8.23 (*s*, 1H), 8.20 (*bs*, 2H) 8.11–8.06 (*m*, 4H), 7.78 (*d*, *J* = 8.3 Hz, 2H), 7.68 (*s*, 1H), 6.98 (*dd*, *J* = 7.45, 5.9 Hz, 1H); ^{13}C-NMR (DMSO-d_6, 125 MHz): 167.91, 154.07, 151.79, 138.16, 135.45, 134.38, 128.45, 127.80, 126.06, 125.58, 125.31, 123.16, 106.70, 15.19; HRMS Calcd. for $C_{19}H_{12}F_3N_3OS$: *m/z* 387.0653; Found 388.078 $[M+H]^+$.

In vitro *MTT assay*

Biological assessment of all synthesized compounds was performed using the standard MTT test to investigate antiproliferative activity against A549, MCF7, DU145, and MCF10 cells. First, 10% FBS was utilized to develop these cell lines. In a 96-well plate, precisely 4×10^3 cells were suspended in MEM and exposed to 5% CO_2 for the duration of the experiment. The cancerous cells were incubated in the culture mix containing all eight synthesized compounds for 72 h. A fresh solution of MTT was introduced to each well, and the cells were subsequently incubated for four hours at 37 °C [35]. Utilizing a multimode reader acquired from Synergy Mx, BioTek, the absorbance at 492 nm was determined to calculate the MTT decrease.

In vitro *enzymatic assay*

The Kinase Glo Plus luminescence kinase assay set performed an enzymatic test on all synthesized compounds *in vitro*. For 45 min, this enzymatic experiment was run at 30 °C. Then, 0.2 mg/mL enzyme-substrate (Poly(Glu, Tyr)), 40 mM Tris, 25 ng kinase, 10 mM $MgCl_2$, 10 µM ATP, 0.1 mg/mL BSA, 1 mM, and DTT pH = 7.4 are all included in the 50 µL reaction mixture used in this test. To achieve a final concentration of 1% in the DMSO solution, 5 µL of every sample solution was individually added to a 45 µL reaction mixture after the molecules had been dissolved in a 10% DMSO solvent. A 50 µL of the Promega Kinase-Glo Plus Luminescence Kinase assay reagent was added to each reaction well after the enzymatic reaction. After that, the plate was left to sit at ambient temperature in a dark room for 15 min. A microplate reader called Spectra Max was used to measure the luminescence signal. The amount of ATP fluorescence is negatively correlated with the level of kinase activity. Graph Pad Prism 8.0 software was used to create a sigmoidal dose-response curve, and nonlinear regression analysis was used to get the IC_{50} values. For each concentration, three separate batches of the tests were conducted.

DPPH assay

The previously reported DPPH assay was utilized to evaluate the free radical scavenging activity of the tested compounds [36]. The compounds were prepared in methanol at concentrations ranging from 0 to 25 µg/mL. For each test, 2.5 mL of the compound solution at three different concentrations was mixed with 1 mL of a 0.3 mM DPPH solution in ethanol. Additionally, 1 mL of methanol was added to the mixture, which was then incubated in the dark at room temperature for 30 min. The absorbance was measured at 518 nm. The blank solution contained 2.5 mL of the test compound and 1 mL of methanol, while the negative control consisted of 1 mL of DPPH solution combined with 2.5 mL of methanol. The percentage of antioxidant activity was calculated using Eq. (1);

$$\%\text{Inhibition} = \frac{A_A - A_B}{A_B} \times 100\% \quad (1)$$

where A_B is the blank sample absorption and A_A is the test sample's absorption. The percentage inhibition value was calculated and compared with that of ascorbic acid as a reference.

Computational methods

Ligand structure preparation. The two-dimensional (2D) chemical structures of **5**(**a**–**h**) were sketched using ACD/ChemSketch software [37]. Prior to the study, the molecular structures and IUPAC nomenclature of the compounds were confirmed using the PubChem® database (https://pubchem.ncbi.nlm.nih.gov/). The structures were then converted from the .cdx file format to the .sdf MDL MOL format as a single file using OpenBabel 2.4.1 software. The energy of the ligand was minimized to prepare it for docking studies.

***In-silico* drug-likeness and ADMET.** The drug-likeness and ADME properties of the newly synthesized compounds were predicted using SwissADME (http://www.swissadme.ch/), an online web server. Drug-likeness, commonly known as Lipinski's rule of

five, is crucial for assessing a molecule's potential to be an orally active drug. This rule was established to predict the pharmacokinetic characteristics of novel therapeutic candidates. According to the rule, a compound should have a molecular weight below 500, a log P value, no more than 5 hydrogen bond donors, and hydrogen bond acceptors not exceeding 10. The pKCSM web server (https://biosig.lab.uq.edu.au/pkcsm/) is specifically developed to predict the ADMET properties of small molecules. It employs machine learning algorithms trained on experimental data to assess these characteristics. By analyzing the structural features of small compounds, these algorithms create predictive models that accurately classify substances based on their pharmacokinetic and toxicological profiles [38]. In this study, the server was utilized to predict toxicity.

Molecular docking study. Molecular docking experiments were performed on synthesized drugs that target the crystal structure of the human EGFR with PDB code 1M17. The molecules were synthesized with LigPrep, and the protein structure was analyzed according to prior research techniques. Docking was done inside the active site of the EGFR utilizing AutoDock Vina 1.5.7 software [39-40]. The QikProp module was used to analyze drug-likeness parameters, while the pkCSM server was used for *in silico* ADMET studies. The crystal structure of the EGFR protein was retrieved from the Protein Data Bank (https://www.rcsb.org/) and subsequently processed. Protein preparation involved selecting the chain containing the relevant amino acids for the co-crystallized ligand, (2R)-2-(1-oxo-1,3-dihydro-2*H*-isoindol-2-yl)-2-phenyl-*N*-(1,3-thiazol-2-yl)acetamide (57N). Non-essential components such as additional chains, heteroatoms, and water molecules were removed from the structure. The binding site was identified based on the co-crystal structure of the native ligand, with dimensions set at x-center = −23.723, y-center = 31.599, and z-center = 12.231, maintaining a uniform box size of 50 (Fig. 2). The energy range was adjusted to 4. Molecular docking was conducted using AutoDock Vina 1.5.7 software to analyze the interactions between all hydrazone analogs and the EGFR protein. AutoDock Vina is an advanced docking tool that incorporates a gradient-based local search genetic algorithm for enhanced accuracy. The ligand-protein interactions were visualized using BIOVIA Discovery Studio 2021. These interactions resulted in binding energy calculations and were analyzed in both 2D and 3D representations.

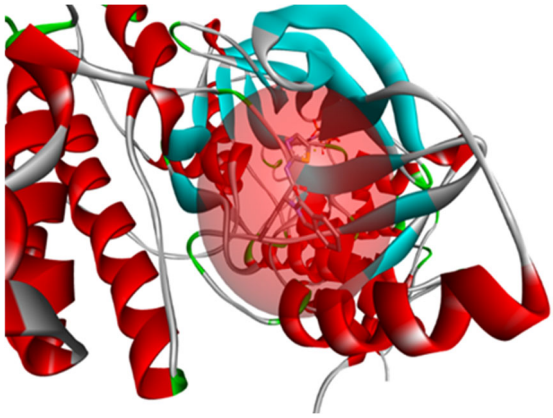

Fig 2. The binding cavity is selected around the native co-crystal ligand

Docking process validation. The docking method was validated by calculating the root mean square deviation (RMSD) value through the superimposition of the hydrazone derivatives onto the native co-crystallized ligand (57N). This analysis was conducted using PyMOL 2.6 software (https://pymol.org/).

Molecular dynamics simulations. Derivatives with good docking scores and potential *in vitro* cytotoxic activity were further evaluated by a molecular dynamics (MD) simulation over 100 ns [41]. These MD simulations were performed by using the Desmond program from the Schrodinger software [42]. Each protein-targeted molecule complex was inserted and solvated within an orthorhombic container. Periodic boundary parameters and the TIP4PEW water model were used to generate an adequate simulation setting for the protein-ligand combined form in the solvated box [43]. Na^+ or Cl^- ions were inserted into the simulation environment to generate an overall neutral charge on the protein-ligand complexes [44]. The NPT ensemble was used for energy minimization and relaxing protein-ligand complexes. The complexes were minimized using the most difficult descent approach after progressively exposing the system to 0 to 310 K, with annealing steps occurring every 2000 steps. Then, a system equilibration phase was

carried out for 1000 steps before the start of the final production run [45]. The MD calculations were carried out for 100 ns, with data collected every 100 ps. The system's temperature and pressure remained constant during the simulation processes at 310 K and 1.01325 bar, respectively. The results of MD trajectory analysis were performed with statistical metrics like as RMSD, RMSF, and protein-ligand interactions. Furthermore, the binding free energy was estimated using the MMGBSA method [46]. The binding free energy was calculated by running the Python software thermal MMGBSA.py on the latest fifty images of MD trajectories with a single-step sampling size [47]. The binding free energy was determined using the principle of additivity, where individual energy modules (ΔG_{bind}, ΔG_{bind}Coulomb, ΔG_{bind}Covalent, $\Delta G_{bind}H_{bond}$, ΔG_{bind}Lipo, ΔG_{bind}SolvGB, and ΔG_{bind}vdW) were combined. The calculation of ΔG_{bind} was performed utilizing Eq. (2);

$$\Delta G_{bind} = \Delta G_{MM} + \Delta G_{Solv} - \Delta G_{SA} \quad (2)$$

where ΔG_{bind} is the binding free energy value, ΔG_{MM} is the difference between the free energies of protein-ligand complexes and the total energies of protein and ligand in isolated form, ΔG_{Solv} is the difference in the G_{SA} solvation energies of the protein-ligand complex and the sum of the solvation energies of the receptor and the ligand in the unbound state, and ΔG_{SA} represents the difference in the surface area energies for the protein and ligand.

■ RESULTS AND DISCUSSION

Synthesis

In the present work, benzofuran thiazolyl hydrazones were synthesized by a one-pot multicomponent reaction, forming the thiazole ring and Schiff base functionality. This one-pot multicomponent condensation reaction includes the C–S, C=N, and C–N bonds formation [48-49]. Benzo[*b*]furan-2-carboxaldehyde (**1**) was reacted with **2** in ethanol in the presence of acetic acid as a catalyst to form 2-(benzofuran-2-ylmethylene)hydrazine-1-carbothioamide as respective thiosemicarbazone derivative (**3**) (Schiff base). This intermediate (**3**) was further *in-situ* refluxed with an equimolar quantity of substituted bromoacetophenone **4**(**a**–**h**) in ethanol to synthesize targeted compounds **5**(**a**–**h**) with good yields (86–90%) by Hantzsch thiazole synthesis (Scheme 1). The newly synthesized 2-aminopyridine thiazolyl hydrazones derivatives were characterized and confirmed by FTIR, ^{1}H-NMR, and ^{13}C-NMR mass spectroscopy analysis.

The FTIR of **5**(**a**–**h**) exhibited a characteristic absorption band around 1650 ± 10 cm^{-1}, indicating the presence of the imine (C=N) group. The newly formed thiazolyl ring was confirmed by absorption around 1230 ± 15 cm^{-1}. In ^{1}H-NMR, a singlet peak around δ value

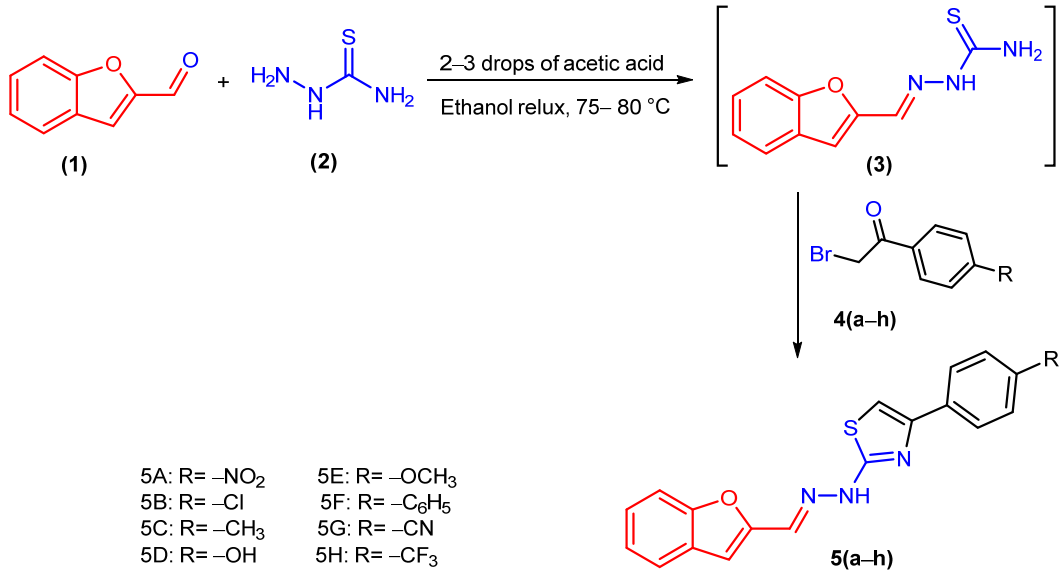

Scheme 1. Synthetic route for targeted compounds of **5** (**a**–**h**)

8.1–8.2 ppm and a broad singlet around δ 12.50 ppm are assigned to amine hydrogen attached to the thiazolyl ring and imine proton attached to the pyridine ring, respectively. The derivative **5h** showed a characteristic absorption band in FTIR spectra at 948 cm^{-1} (C–F stretch), whereas analog **5g** showed absorption at a frequency of 2217 cm^{-1}, confirming the –CN group.

Biological Study

In vitro *anticancer activity*

The MTT assay test was used to assess the antiproliferative activity against the chosen cancer cell lines. Doxorubicin and osimertinib were used as a reference for biological assay. The result of the MTT assay was shown as IC_{50} values in Table 1. Compounds **5a**, **5g**, and **5h** have shown better anticancer activity. Compound **5h** has shown the best antiproliferative activity against A-549, MCF7, and DU145 cells with IC_{50} values of 9.05, 12.03, and 10.01 μM, respectively. We have attempted the structural activity relationship data of the synthesized derivatives. It revealed that compounds **5a** and **5g** with an electron-withdrawing group (NO_2 and CN) on the benzene ring diminished activity against A-549 and MCF7 cell lines. The imine derivatives **5a**, **5g**, and **5h** showed noticeable anticancer activity against A-549 and MCF7 cell lines with an IC_{50} value ranging from 9–12 μM.

In vitro *enzymatic activity assay*

An *in-vitro* test was performed to inhibit the enzymatic activity of the synthesized molecules against wild-type EGFR. Osimertinib was taken as a reference standard. The results are mentioned in Table 2. Among all, compounds **5g** and **5h** demonstrated strong inhibitory activity against wild-type EGFR with an IC_{50} of 2.40 and 1.89 μM, respectively.

DPPH radical scavenging activity

Free radicals have a key role in cancer, cardiovascular, and auto-immune illnesses, as well as aging-related issues, leading to new medical approaches [50]. The scavenging capacity of the produced compounds was evaluated using the previously published DPPH technique. Ascorbic acid was employed as a control. As indicated in Table 3, the compounds **5g** and **5h** were evaluated at concentrations such as 10, 50, and 100 μM, displaying good antioxidant properties. Compound **5g** showed substantial antioxidant activity at a concentration of 100 μM, with a DPPH radical scavenging value of 91.46%.

Table 2. *In vitro* enzymatic inhibitory activity of synthesized molecules against EGFR

Compound	IC_{50} μM[a]
	EGFR inhibition
5g	2.40 ± 0.21
5h	1.89 ± 0.10
Osimertinib (**5i**)	1.35 ± 0.14

[a]The data reported are the mean values from three independent experiments

Table 1. *In vitro* anticancer screening of the synthesized **5**(**a**–**h**) against four different cell lines

Compound	IC_{50} μM[a]				Selectivity index
	A549 (WT EGFR)	MCF7 (WT EGFR)	DU145 (WT EGFR)	MCF10 (Non-special gene type)	
5a	13.57 ± 0.60	10.05 ± 1.90	14.09 ± 1.40	87.23	6.93
5b	54.01 ± 0.20	57.04 ± 0.50	56.08 ± 0.80	ND	-
5c	14.56 ± 1.10	45.67 ± 1.80	55.03 ± 0.60	ND	-
5d	78.06 ± 1.20	70.01 ± 1.50	78.09 ± 0.40	ND	-
5e	60.04 ± 1.20	67.05 ± 0.80	19.07 ± 1.20	ND	-
5f	18.09 ± 0.80	15.03 ± 1.20	24.11 ± 1.60	92.77	4.86
5g	10.08 ± 1.80	13.09 ± 1.40	15.06 ± 0.40	85.64	6.72
5h	9.05 ± 1.90	12.03 ± 1.40	10.01 ± 1.10	78.46	7.57
Osimertinib **(5i)**	8 ± 2.40	-	-	98.45	12.30
Doxorubicin	2.5 ± 1.10	13.7 ± 2.40	11.3 ± 1.70	95.35	10.47

[a]The reported data is based on the mean values of three separate experiments; ND = not determined

Table 3. DPPH antioxidant activity results

Compound	Antioxidant (DPPH radical scavenging activity %) at various concentrations (μM)		
	100	50	10
5g	91.46	94.57	53.26
5h	80.88	81.23	52.38
Ascorbic acid	96.73	92.27	64.75

Computational Study

Druglikeness and ADMET study

The evaluation of synthesized compounds using Lipinski's rule of five and Jorgensen's rule of three is given in (Table 4). The synthesized compounds **5**(**a**–**h**) have molecular weights (MW) ranging from 333.41 to 395.48, all below the 500 thresholds of Lipinski's rule. The number of hydrogen bond donors (donor HB) for all compounds is 1 or 2, within the acceptable limit of 5. Hydrogen bond acceptors (acceptor HB) range from 3.0 to 5.5, also within the acceptable range of 10. Despite this, **5b** and **5c** each have one violation of Lipinski's rule of five due to their QPlogPo/w values exceeding 5. Regarding Jorgensen's rule of three, which assesses solubility, permeability, and metabolic stability, most compounds have QPlogS values below the threshold of −5.7, except for **5c**. The number of primary metabolites (#metab) for the compounds ranges from 0 to 1, well below the threshold of 7. The QPPCaco values, representing cell permeability, are above the threshold of 22 nm/s for all compounds, indicating good permeability. Notably, all compounds exhibit a predicted human oral absorption percentage of 100%, suggesting excellent absorption characteristics. Overall, the compounds comply with Lipinski's rule of five and Jorgensen's rule of three, indicating good drug-likeness and high potential for oral absorption in humans.

The *in silico* ADMET predictions for the synthesized **5**(**a**–**h**) indicate several notable characteristics regarding their pharmacokinetic and toxicity profiles. All compounds exhibit moderate to low water solubility, with **5f** being the least soluble and **5d** the most soluble. All compounds are P-glycoprotein substrates and inhibitors, indicating potential for drug-drug interactions. It also suggests these compounds may be effectively transported across cellular barriers. In terms of distribution, the distribution volume suggests low distribution for most compounds, with **5d** having the highest and **5h** having the lowest values (Table 5). They all show high protein binding with low fractions unbound in human plasma and varying degrees of blood-brain barrier permeability, with **5b** and **5c** having the highest permeability. None of the compounds are substrates for CYP2D6, reducing the risk of interactions with drugs metabolized by this enzyme. Most compounds do not

Table 4. Lipinski's rule of five and Jorgensen rule of three (drug likeliness) of prediction synthesized compounds

Comp ID	Lipinski's rule of five					Jorgensen rule of three				%Human oral absorption
	mol MW	Donor HB	Acceptor HB	QPlogPo/w	Rule of five	QPlogS	#metab	QPPCaco	Rule of three	
5a	364.38	1	5.50	3.65	0	−5.53	3	542.06	0	100
5b	353.83	1	3.00	5.43	1	−5.40	3	4815.71	0	100
5c	333.41	1	3.00	5.25	1	−6.54	4	4813.35	1	100
5d	335.38	2	5.25	3.13	0	−4.30	3	823.59	0	100
5e	349.41	1	5.25	4.44	0	−5.58	3	4570.88	0	100
5f	395.48	1	3.00	4.37	0	−4.99	3	4831.82	0	100
5g	344.39	1	4.50	4.18	0	−4.93	3	999.44	0	100
5h	387.38	1	3.00	4.92	0	−5.40	3	4813.36	0	100

Lipinski's rule of five: MW < 500, log Po/w < 5, donor HB ≤ 5, accept HB ≤ 10; Jorgensen's rule of three: QPlogS < -5.7, QPPCaco > 22 nm/s, # primary metabolites < 7; percent human oral absorption on 0 to 100% scale (> 80% is high < 25% is poor)

Table 5. *In silico* ADMET prediction of the synthesized compounds

Parameters		5A	5B	5C	5D	5E	5F	5G	5H
Absorption	Water solubility (log mol/L)	−5.041	−5.349	−5.221	−4.678	−4.785	−6.392	−4.942	−5.498
	P-glycoprotein substrate	Yes	Yes	Yes	Yes	Yes	Yes	Yes	Yes
	P-glycoprotein I inhibitor	Yes	Yes	Yes	Yes	Yes	Yes	Yes	Yes
	P-glycoprotein II inhibitor	Yes	Yes	Yes	Yes	Yes	Yes	Yes	Yes
Distribution	VDss (human) (L/kg)[a]	−0.097	0.124	0.137	−0.053	0.155	0.46	0.019	0.164
	Fraction unbound (human) (Fu)	0.061	0.073	0.083	0.095	0.068	0.165	0.078	0.061
	BBB permeability (log BB)[b]	−0.791	0.537	0.550	−0.508	0.409	0.513	-0.447	0.497
Metabolism	CYP2D6 substrate	No	No	No	No	No	No	No	No
	CYP3A4 substrate	Yes	Yes	Yes	Yes	Yes	Yes	Yes	Yes
	CYP1A2 inhibitor	Yes	Yes	Yes	Yes	Yes	Yes	Yes	Yes
	CYP2C19 inhibitor	Yes	Yes	Yes	Yes	Yes	Yes	Yes	Yes
	CYP2C9 inhibitor	Yes	Yes	Yes	Yes	Yes	Yes	Yes	No
	CYP2D6 inhibitor	No	No	No	No	Yes	No	No	No
	CYP3A4 inhibitor	Yes	No	No	No	No	Yes	No	Yes
Excretion	Total clearance (mL/min/kg)	0.298	0.263	0.338	0.162	0.31	0.348	0.362	0.315
	Renal OCT2 substrate	No	Yes	Yes	Yes	Yes	No	Yes	Yes
Toxicity	AMES toxicity	Yes	Yes	Yes	Yes	Yes	Yes	Yes	Yes
	Max. tolerated dose (human) (log mg/kg/day)[c]	0.165	−0.131	−0.145	−0.15	−0.143	0.73	−0.218	−0.213
	hERG-I inhibitor	No	No	No	No	No	No	No	No
	Oral rat acute toxicity (LD_{50}, mol/kg)	3.052	2.074	2.072	2.071	2.199	2.179	2.074	2.164
	Oral rat chronic toxicity (LOAEL, mg/kg bw/day)	1.158	0.702	0.829	0.949	1.172	1.026	0.883	0.618

[a]VDss is considered low if below 0.71 L/kg and high if above 2.81 L/kg; [b]For a given compound a logBB > 0.3 considered to readily cross the blood brain barrier while molecule with logBB < −1 are poorly distributed to the brain; [c]For a given compound maximum tolerated dose of less than or equal to 0.447 log(mg/kg/day) is considered low and high if >0.477 log(mg/kg/day)

inhibit CYP2D6 (except **5e**), minimizing potential drug-drug interactions involving this enzyme. Several compounds (**5b**, **5c**, **5d**, **5e**, and **5g**) do not inhibit CYP3A4, reducing the risk of interactions with drugs metabolized by this enzyme. The compounds exhibit moderate total clearance rates, and most are substrates for renal OCT2, affecting renal excretion. Toxicity profiles reveal that all compounds tested positive for AMES toxicity, suggesting potential mutagenic effects. The maximum tolerated doses are generally low, with S6 showing the highest tolerance. None of the compounds inhibit the hERG channel, indicating a lower risk of cardiotoxicity. In summary, the synthesized compounds exhibit favorable safety profiles in terms of blood-brain barrier permeability, lack of CYP2D6 interaction, non-inhibition of hERG channels, and acceptable acute and chronic toxicity values. However, concerns regarding P-glycoprotein interaction and AMES toxicity need further investigation to ensure comprehensive safety in drug development.

Molecular Docking Results

To better understand the biological processes behind newly synthesized nitrobenzene thiazolyl hydrazone derivatives, we assessed their binding affinity and interaction mode at the EGFR protein binding site. The EGFR protein was chosen as the docking target because of its clearly defined crystal structure and high affinity for its 57N ligand. The docking study found the compounds with the lowest binding energy, the most hydrogen bonds, and the shortest bond lengths. The bond length, bonding type, and binding energy were shown in both 2D and 3D forms [51]. The docking results for the synthesized compounds against EGFR protein are summarized in Table 6, with docking scores indicating

Table 6. Docking score of the synthesized compound in the active site of EGFR protein

Compound	Docking score (kcal/mol)
5a	−7.361
5b	−6.958
5c	−6.827
5d	−6.944
5e	−6.962
5f	−6.853
5g	−7.445
5h	−7.223
Osimertinib (**5i**)	−7.900

the binding score of each compound. A more negative score signifies stronger interactions with the enzyme.

The docking scores of the compounds range from −7.445 to −6.827 kcal/mol. Among these scores, compounds **5a**, **5g**, and **5h** exhibit particularly promising docking affinities with values of −7.361, −7.445, and −7.223 kcal/mol, respectively. The promising docking scores of **5g** and **5h** indicate a strong potential for binding and modulation of EGFR activity. These compounds also demonstrate significant efficacy in inhibiting EGFR enzyme function, as evidenced by their respective IC_{50} values of 2.40 and 1.89 μM, highlighting their potential as lead compounds for further development in targeted cancer therapy. The 2D and 3D binding poses of compounds **5g** and **5h** are visually represented in Fig. 3, and the 2D non-covalent interactions of all compounds against the EGFR protein can be found in Fig. S33-S39. Both compounds do not involve direct hydrogen bond interactions but exhibit interactions with the active site residues of EGFR through van der Waals forces of interaction. These include Leu694, Gly695, Glu697, Phe699, Val702, Leu764, Thr766, Leu768, Met769, Gly772, Thr830, and Asp831. Such interactions are crucial for stabilizing the ligand-protein complex and facilitating the inhibition of EGFR activity.

MD Simulations

The MD simulations of **5g** and **5h** with EGFR receptor were the focus of the MD simulation analysis of the docked complexes, which was carried out over 100 ns using the Desmond software. Numerous parameters, i.e., RMSD, root mean square fluctuations (RMSF), changing

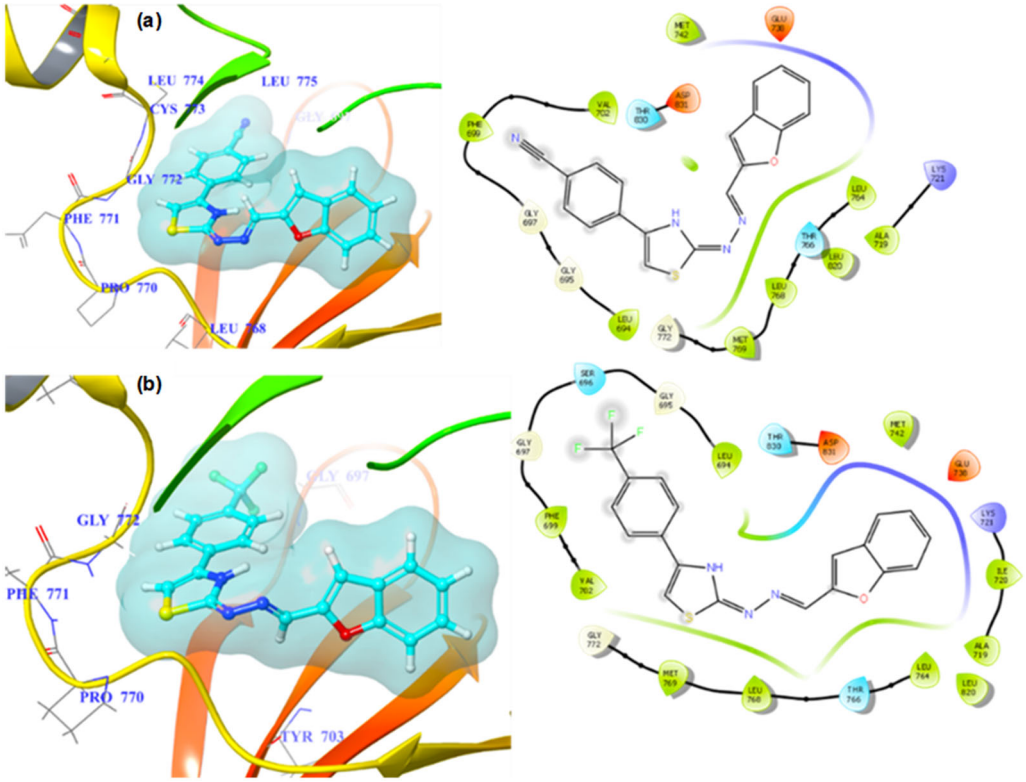

Fig 3. The 2D and 3D molecular interaction of compounds (a) **5g** and (b) **5h** against EGFR protein

protein-ligand interactions throughout time, and binding free energy computations based on the MD trajectory's final frames, were used extensively to assess the resultant MD trajectory. A thorough investigation of the dynamic behavior of the protein-ligand complexes over the 100 ns simulation period was made possible by the MD simulation of compounds **5g** and **5h** with EGFR kinase. The study included an in-depth investigation of how the binding interactions and free energy of compounds **5g** and **5h** with EGFR kinase develop in a realistic physiological simulation. Parameters such as RMSD and RMSF provided information on the complex's general stability and fluctuations, whilst changing protein-ligand contacts provided a dynamic perspective of the interactions throughout the simulation. Additionally, binding free energy calculations help to understand the thermodynamic features of ligand-protein binding.

Fig. 4 shows the RMSD curve of simulated complexes. After the first 20 ns of simulation, the RMSD profile of the 1M17-**5h** complex showed a continuous trend with a centered graph. Fig. 4(a) shows that the 1M17-**5h** complex's RMSD values went up slightly. Furthermore, the complex exhibited increased dispersion in RMSD before around 20 ns, which can be attributed to the complex's first stabilization stages. The post-20 ns centered graph represents a time in which the complex gained a more stable conformation, resulting in a more uniform RMSD pattern. The first scattering detected before this period might indicate structural or conformational changes as the complex first interacts with the protein target. Once stabilization is achieved, the RMSD readings show a more regulated and centered behavior, indicating that the 1M17-**5h** complex is in a generally stable configuration throughout this simulation period. The RMSD analysis of the backbone Cα of EGFR and the bound molecule **5h** in Fig. 4(a) with sky-blue and green colors, respectively, demonstrates a constant alignment throughout the simulation with low scattering. The individual structures (1M17 and **5h**) had lower RMSD than their complex form (1M17-**5h**). The RMSD of **5h** showed a continuous curve with RMSD value below ~2 Å. However, a substantial variance was noted in the early 20 ns. RMSD study of the backbone Cα revealed significant scattering ranging from ~40 to ~50 ns. Individual structures had stable and reduced RMSD values with insignificant variation compared to their complex form, indicating that both structures maintained their structural arrangement with minor fluctuations during the simulation.

In Fig. 4(b), the RMSD profile of the 1M17-**5g** complex, along with the backbone Cα and compound **5g**, was analyzed. All components in the 1M17-**5g** complex have RMSD values below ~3.5 Å. Notably, compound **5g** had the most stable conformation in its bound state within the EGFR binding pocket, and the RMSD plot for this derivative was continuously centered with negligible dispersion. The centered RMSD plot for compound **5g** from ~0.5 Å to ~1 Å revealed a relatively stable conformation when coupled to the EGFR protein. The RMSD profiling of the MD trajectory for both complexes

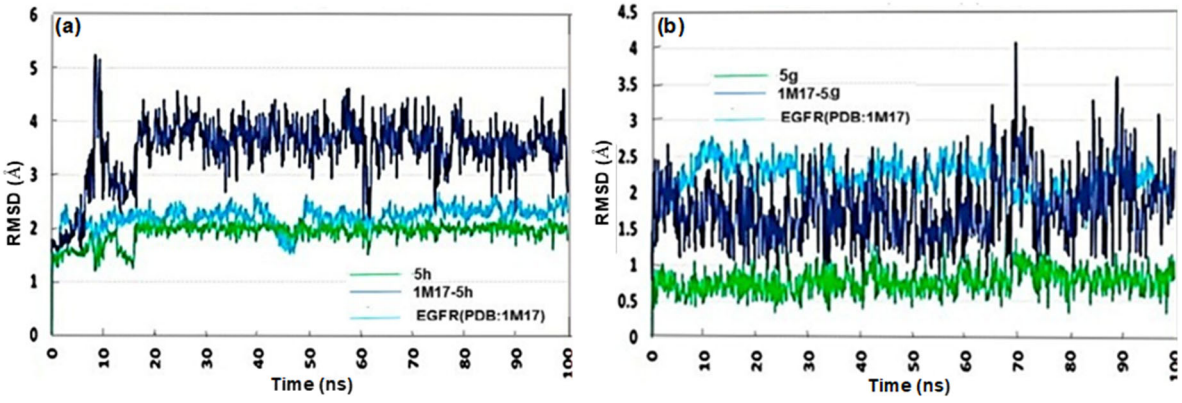

Fig 4. RMSD profile for scaffold protein, protein-ligand complex, and ligand structure from simulated complexes of (**a**) 1M17-**5h** and (**b**) 1M17-**5g** over 100 ns MD simulation

revealed important information on the structural dynamics and stability of the 1M17-**5h** and 1M17-**5g** complexes. The slight discrepancies in the RMSD values and plot, as seen in Fig. 4, necessitated more investigation to determine and recognize the underlying reasons for these RMSD values. The structural shift seen in the RMSD figure might be attributable to residual changes in amino acid residues involved in drug binding or the protein's overall structure. To go further into the specifics of these residual oscillations and get more thorough insights, RMSF analysis was performed on the simulated MD trajectory. The RMSF profiling was useful for estimating the residual variations of individual amino acid residues in the EGFR protein during the 100 ns MD simulation. The RMSF plot for both simulated complexes is shown in Fig. 5. The RMSF study of the 1M17-**5h** complex found minor alterations in all amino acid residues, with values typically below ~3 Å. The 1M17-**5g** complex followed a similar RMSF trend. The RMSF profiling data showed that amino acid residues migrated in predictable ways over the 100 ns MD simulation. The small fluctuations in RMSF values indicated that the amino acid residues involved in the interaction with compounds **5g** and **5h** exhibited exceptionally stable and controlled dynamics during the 100 ns MD simulation. This coordinated mobility of residues indicates a well-mannered and stable protein-ligand complex, with binding interactions contributing to system stability. Overall, RMSF profiling confirmed that residue variations are not responsible for the conformational divergence of complexes seen in the RMSD.

Further examination of changing protein-ligand interactions during the simulation was conducted to determine their function in the conformational variation found in RMSD. This approach involves determining the proportion of binding contacts and the consistency of interactions between residues and bounded compounds during the 100 ns MD trajectory. Fig. 6 shows the results charts from this investigation. These charts offered useful information on how the protein-ligand interactions changed during the MD simulation run and how they altered the complex structure The proportion of binding contacts and the uniformity of interaction were used to assess if individual residues contributed to the stability of the complex or whether there are transitory interactions that may have influenced the noticed conformational aberrations in the RMSD plot. Fig. 6(a) and 6(b) show that Phe856 consistently binds to compound **5h** in the interaction analysis of the 1M17-**5h** complex. Phe856 made the most hydrogen bonds in comparison to other residues. This conclusion is consistent with the findings from the docking investigation, where the identical residue, Phe856, formed a π-π T-shaped contact with **5h**. The continuous binding of Phe856 to compound **5h**, as shown by the proportion of hydrogen bonds, revealed that this residue played an essential role in stabilizing the complex across the 100 ns simulation. The docking investigation found

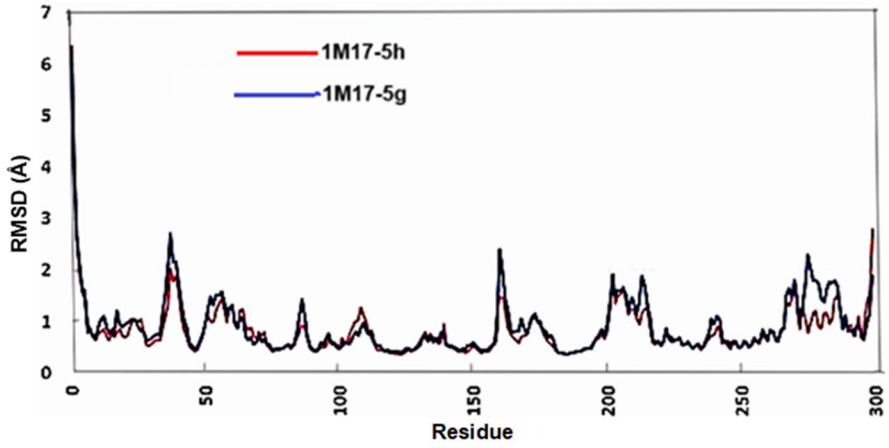

Fig 5. RMSF profile for backbone protein from simulated (**a**) 1M17-**5h** and (**b**) 1M17-**5g** complexes over 100 ns MD simulation

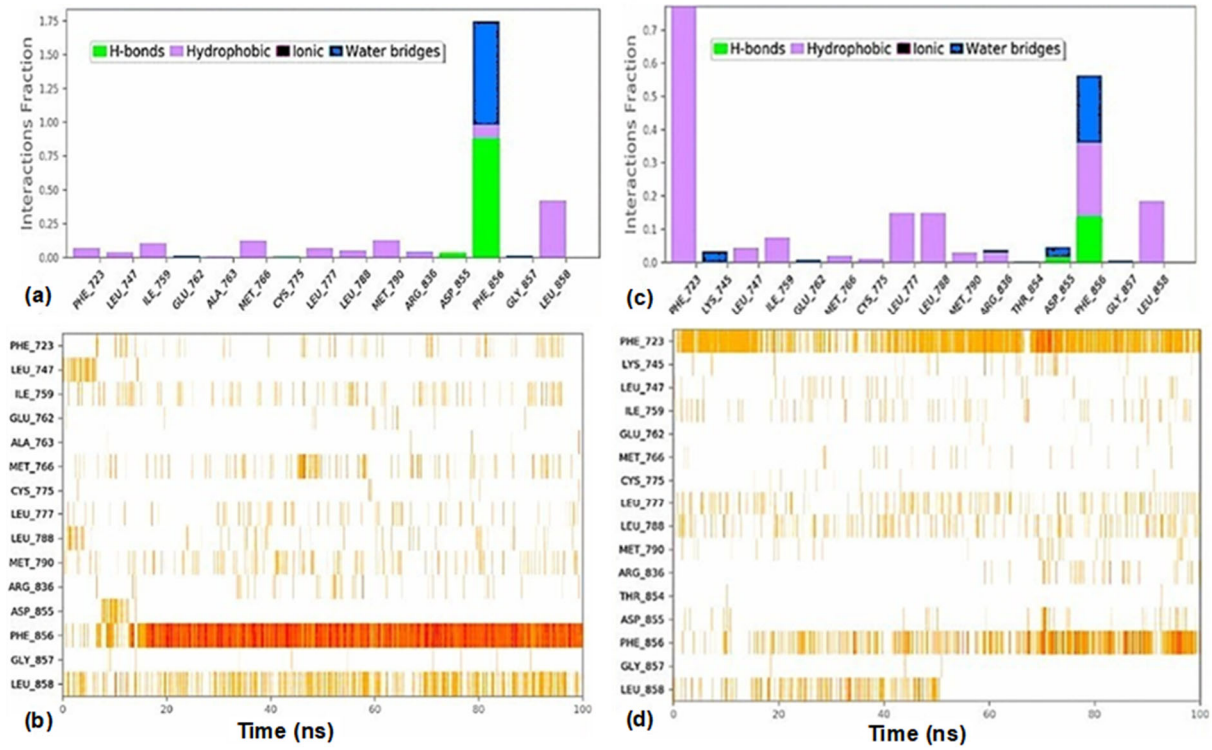

Fig 6. Protein-ligand contacts from simulated (**a**–**b**) 1M17-**5h** and (**c**–**d**) 1M17-**5g** complexes over 100 ns MD simulation

a π-π T-shaped connection, which supports the idea that Phe856 has constant and unique interactions with compound **5h**. In the instance of the 1M17-**5h** complex, whereas Phe856 was shown to contribute to binding interactions regularly, Leu858 was also discovered to contribute to complex stability. Leu858's involvement revealed that many residues worked together to provide stability to the protein-ligand complex through binding interactions. The study of protein-ligand interactions in Fig. 6(c–d) revealed that Phe723 consistently binds to compound **5g**. In addition, compound **5h** formed hydrogen bonds with Asp855 and Phe856. This showed that these residues substantially stabilized the complex by forging persistent connections with **5h**. Particularly, the majority of the amino acid residues discovered during the binding interaction research following docking helped create protein-ligand interactions during the MD simulation. This alignment of docking and MD simulation findings confirmed the trustworthiness of the binding interactions discovered using computational approaches. These particular acids might contribute to the protein-ligand complexes' stability throughout the 100 ns MD simulation. This information improves the usability of the MD simulation findings and gives a more detailed picture of the molecular connections that control the behavior of these complexes over time.

The binding free energy of the simulated complexes was analyzed using the MD trajectory's end frames, and the energies were calculated using the MMGBSA technique. Fig. 6 shows a graph of the obtained data. Interestingly, both complexes have virtually comparable calculated interaction energies, such as ΔG_{bind}, ΔG_{bind}Coulomb, ΔG_{bind}Covalent, ΔG_{bind}Hbond, ΔG_{bind}Lipo, ΔG_{bind}SolvGB, and ΔG_{bind}vdW. Interestingly, both complexes showed high ΔG_{bind}Coulomb energies. The identical patterns in interaction energies found in both complexes, as shown in Fig. 7, provide credence to the notion that protein-ligand interactions stay stable during the 100 ns MD simulation. Strong ΔG_{bind}Coulomb energies with large negative values indicate strong electrostatic interactions within complexes. This extensive investigation of binding free energy yielded new

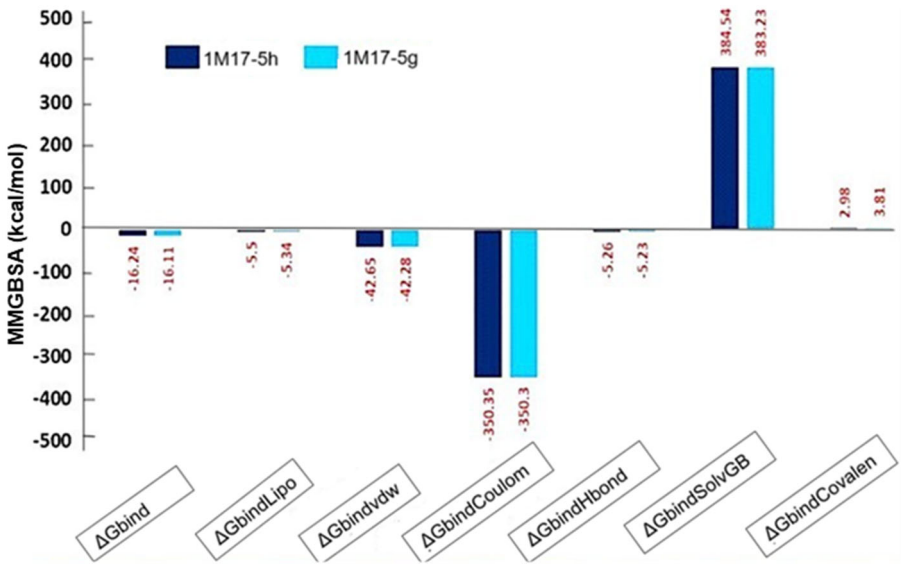

Fig 7. Graphical representation of calculated binding free energy profile of simulated complexes

quantitative insights into the thermodynamic stability of protein-ligand complexes. The overall results from MD simulations provided a more thorough insight into the binding modes, affinity, type of interactions, and general stability of the compounds inside the EGFR binding site. This real-time simulation verified and expanded upon the findings of the first docking and *in vitro* cytotoxicity investigation. This knowledge is critical for improving the future design of these molecules as possible as anticancer medicines. As a result, running molecular dynamics simulations was a natural and significant next step in investigating compounds **5h** and **5g**. This helped thoroughly assess their efficacy as anticancer drugs targeting EGFR.

■ CONCLUSION

We synthesized novel benzofuran thiazolyl thiazolyl hydrazones using a pharmacophore-based drug-design method via a one-pot multicomponent reaction. Various analytical techniques were utilized to determine the structures of novel molecules. The synthesized derivatives were assessed for antiproliferative activity against MCF7, A549, DU145 cancer, and MCF10 normal cell lines. Among all, **5g** and **5h** could inhibit EGFR activity at concentrations ~1.89–2.40 μM. As per MTT assay results, all the derivatives demonstrated moderate (9 μM) to better (15 μM) inhibition as compared to reference drugs. Compounds **5g** and **5h** showed the most potent inhibition activity against EGFR and good antioxidant activity. In molecular docking investigations, all ligands in their conformational state were adequately anchored into the pocket of the wild EGFR enzymes. Thus, all these findings of this study show that benzofuran thiazolyl hydrazones, specifically **5g** and **5h**, have significant anticancer potential and might be further optimized for the design and development of new EGFR inhibitors.

■ ACKNOWLEDGMENTS

This work was supported by regular institutional funding, and no additional grants were obtained.

■ CONFLICT OF INTEREST

The authors declared no conflict of interest.

■ AUTHOR CONTRIBUTIONS

Sonali Sandeep Shinde–Conceptualization, methodology, validation, investigation, data curation, project administration. Jaydeo Tirthraj Kilbile–Methodology. Sachin Shivling Bhusari and Pravin Shridhar Wakte–Critical analysis and cross-verification of the docking results and all authors reviewed the manuscript.

■ REFERENCES

[1] Siegel, R.L., Kratzer, T.B., Giaquinto, A.N., Sung, H., and Jemal, A., 2025, Cancer statistics, *Ca-Cancer J. Clin.*, 75 (1), 10–45.

[2] Wee, P., and Wang, Z., 2017, Epidermal growth factor receptor cell proliferation signaling pathways, *Cancers*, 9 (5), 52.

[3] Yu, H., 2023, Optimising Cancer Therapeutics: An *In Vitro* and *In Silico* Approach, *Dissertation*, Aston University, UK.

[4] Mejía-Caballero, A., Salas-Villagrán, V.A., Jiménez-Serna, A., and Farrés, A., 2021, Challenges in the production and use of probiotics as therapeutics in cancer treatment or prevention, *J. Ind. Microbiol. Biotechnol.*, 48 (9-10), kuab052.

[5] Yaron-Barir, T.M., Joughin, B.A., Huntsman, E.M., Kerelsky, A., Cizin, D.M., Cohen, B.M., Regev, A., Song, J., Vasan, N., Lin, T.Y., Orozco, J.M., Schoenherr, C., Sagum, C., Bedford, M.T., Wynn, R.M., Tso, S.C., Chuang, D.T., Li, L., Li, S.S.C., Creixell, P., Krismer, K., Takegami, M., Lee, H., Zhang, B., Lu, J., Cossentino, I., Landry, S.D., Uduman, M., Blenis, J., Elemento, O., Frame, M.C., Hornbeck, P.V., Cantley, L.C., Turk, B.E., Yaffe, M.B., and Johnson, J.L., 2024, The intrinsic substrate specificity of the human tyrosine kinome, *Nature*, 629 (8014), 1174–1181.

[6] Raghu, M.S., Swarup, H.A., Shamala, T., Prathibha, B.S., Kumar, K.Y., Alharethy, F., Prashanth, M.K., and Jeon, B.H., 2023, Design, synthesis, anticancer activity, and docking studies of novel quinazoline-based thiazole derivatives as EGFR kinase inhibitors, *Heliyon*, 9 (9), e20300.

[7] Wang, S., Song, Y., and Liu, D., 2017, EAI045: The fourth-generation EGFR inhibitor overcoming T790M and C797S resistance, *Cancer Lett.*, 385, 51–54.

[8] Milik, S.N., Lasheen, D.S., Serya, R.A., and Abouzid, K.A., 2017, How to train your inhibitor: Design strategies to overcome resistance to epidermal growth factor receptor inhibitors, *Eur. J. Med. Chem.*, 142, 131–151.

[9] Das, D., and Hong, J., 2019, Recent advancements of 4-aminoquinazoline derivatives as kinase inhibitors and their applications in medicinal chemistry, *Eur. J. Med. Chem.*, 170, 55–72.

[10] El-Sherief, H.A.M., Youssif, B.G.M., Abdelazeem, A.H., Abdel-Aziz, M., and Abdel-Rahman, H.M., 2019, Design, synthesis and antiproliferative evaluation of novel 1,2,4-triazole/Schiff base hybrids with EGFR and B-RAF inhibitory activities, *Anti-Cancer Agents Med. Chem.*, 19 (5), 697–706.

[11] Hashem, H.E., Amr, A.E.G.E., Nossier, E.S., Anwar, M.M., and Azmy, E.M., 2022, New benzimidazole-, 1,2,4-triazole-, and 1,3,5-triazine-based derivatives as potential EGFRWT and EGFRT790M inhibitors: Microwave-assisted synthesis, anticancer evaluation, and molecular docking study, *ACS Omega*, 7 (8), 7155–7171.

[12] Kardile, R.A., Sarkate, A.P., Lokwani, D.K., Tiwari, S.V., Azad, R., and Thopate, S.R., 2023, Design, synthesis, and biological evaluation of novel quinoline derivatives as small molecule mutant EGFR inhibitors targeting resistance in NSCLC: *In vitro* screening and ADME predictions, *Eur. J. Med. Chem.*, 245, 114889.

[13] Karnik, K.S., Sarkate, A.P., Tiwari, S.V., Azad, R., and Wakte, P.S., 2021, Free energy perturbation guided synthesis with biological evaluation of substituted quinoline derivatives as small molecule L858R/T790M/C797S mutant EGFR inhibitors targeting resistance in non-small cell lung cancer (NSCLC), *Bioorg. Chem.*, 115, 105226.

[14] Jiao, X., Zhang, Q., Zhang, Y., Shao, J., Ding, L., Tang, C., and Feng, B., 2022, Synthesis and biological evaluation of new series of quinazoline derivatives as EGFR/HER2 dual-target inhibitors, *Bioorg. Med. Chem. Lett.*, 67, 128703.

[15] Ibrahim, M.T., Uzairu, A., Uba, S., and Shallangwa, G.A., 2021, Design of more potent quinazoline derivatives as EGFR WT inhibitors for the treatment of NSCLC: A computational approach, *Future J. Pharm. Sci.*, 7 (1), 140.

[16] Ahmed, N.M., Youns, M.M., Soltan, M.K., and Said, A.M., 2021, Design, synthesis, molecular modeling and antitumor evaluation of novel indolyl-

pyrimidine derivatives with EGFR inhibitory activity, *Molecules*, 26 (7), 1838.

[17] Al-Anazi, M., Khairuddean, M., Al-Najjar, B.O., Alidmat, M.M., Nik Mohamed Kamal, N.N.S., and Muhamad, M., 2022, Synthesis, anticancer activity and docking studies of pyrazoline and pyrimidine derivatives as potential epidermal growth factor receptor (EGFR) inhibitors, *Arabian J. Chem.*, 15 (7), 103864.

[18] Farghaly, T.A., Abbas, E.M., Al-Soliemy, A.M., Sabour, R., and Shaaban, M.R., 2022, Novel sulfonyl thiazolyl-hydrazone derivatives as EGFR inhibitors: Design, synthesis, biological evaluation and molecular docking studies, *Bioorg. Chem.*, 121, 105684.

[19] Al-Wahaibi, L.H., El-Sheref, E.M., Hassan, A.A., Bräse, S., Nieger, M., Youssif, B.G.M., Ibrahim, M.A., and Tawfeek, H.N., 2023, Synthesis and structure determination of substituted thiazole derivatives as EGFR/BRAFV600E dual inhibitors endowed with antiproliferative activity, *Pharmaceuticals*, 16 (7), 1014.

[20] Xu, Z., Xu, D., Zhou, W., and Zhang, X., 2022, Therapeutic potential of naturally occurring benzofuran derivatives and hybrids of benzofurans with other pharmacophores as antibacterial agents, *Curr. Top. Med. Chem.*, 22 (1), 64–82.

[21] Scibetta, S., Miceli, M., Iuliano, M., Stefanuto, L., Carbone, E., Piscopo, P., Petrozza, V., Romeo, G., Mangino, G., Calogero, A., Gasperi, T., and Rosa, P., 2024, *In vitro* evaluation of the antioxidant capacity of 3,3-disubstituted-3*H*-benzofuran-2-one derivatives in a cellular model of neurodegeneration, *Life*, 14 (4), 422.

[22] El-Khouly, O.A., Henen, M.A., El-Sayed, M.A.A., Shabaan, M.I., and El-Messery, S.M., 2021, Synthesis, anticancer and antimicrobial evaluation of new benzofuran based derivatives: PI3K inhibition, quorum sensing and molecular modeling study, *Bioorg. Med. Chem.*, 31, 115976.

[23] Bendi, A., Sirija, M.R., Bhathiwal, A.S., Chinmay, C., Chauhan, V., and Tiwari, A., 2024, Exploring the potential therapeutic role of benzofuran derivatives in cancer treatment, *J. Mol. Struct.*, 1317, 139121.

[24] Mphahlele, M.J., Maluleka, M.M., Parbhoo, N., and Malindisa, S.T., 2018, Synthesis, evaluation for cytotoxicity and molecular docking studies of benzo[*c*]furan-chalcones for potential to inhibit tubulin polymerization and/or EGFR-tyrosine kinase phosphorylation, *Int. J. Mol. Sci.*, 19 (9), 2552.

[25] Petrou, A., Fesatidou, M., and Geronikaki, A., 2021, Thiazole ring—A biologically active scaffold, *Molecules*, 26 (11), 3166.

[26] Sanachai, K., Aiebchun, T., Mahalapbutr, P., Seetaha, S., Tabtimmai, L., Maitarad, P., Xenikakis, I., Geronikaki, A., Choowongkomon, K., and Rungrotmongkol, T., 2021, Discovery of novel JAK2 and EGFR inhibitors from a series of thiazole-based chalcone derivatives, *RSC Med. Chem.*, 12 (3), 430–438.

[27] Al-Salmi, F.A., Alrohaimi, A.H., El Behery, M., Megahed, W., Abu Ali, O.A., Elsaid, F.G., Fayad, E., Mohammed, F.Z., and Keshta, A.T., 2023, Anticancer studies of newly synthesized thiazole derivatives: Synthesis, characterization, biological activity, and molecular docking, *Crystals*, 13 (11), 1546.

[28] Verma, G., Marella, A., Shaquiquzzaman, M., Akhtar, M., Ali, M.R., and Alam, M.M., 2024, A review exploring biological activities of hydrazones, *J. Pharm. BioAllied Sci.*, 6, 69–80.

[29] Al-Hazmi, G.H., 2023, *In vitro* biological evaluation of some synthesized novel 5-substituted-2-(substituted)hydazineyl-1,3-thiazolidin-4-ones, *Russ. J. Bioorg. Chem.*, 49 (5), 1000–1013.

[30] Rathod, S.S., Shinde, S.S., Choudhari, P.B., Dhavale, R.P., and Sarkate, A.P., 2024, "Computational and Experimental Approaches to Decipher the Complexity of Diseases" in *Systems Biology Approaches: Prevention, Diagnosis, and Understanding Mechanisms of Complex Diseases*, Eds. Joshi, S., Ray, R.R., Nag, M., and Lahiri, D., Springer Nature Singapore, Singapore, 393–413.

[31] Shinde, S.S., Ahmed, S., Malik, J.A., Hani, U., Khanam, A., Ashraf Bhat, F., Ahmad Mir, S., Ghazwani, M., Wahab, S., Haider, N., and Almehizia, A.A., 2023, Therapeutic delivery of tumor suppressor miRNAs for breast cancer treatment, *Biology*, 12 (3), 467.

[32] Rathod, S., Shinde, S., Choudhari, P., Sarkate, A., Chaudhari, S., and Shingan, A., 2025, Exploring binding potential of two new indole alkaloids from *Nauclea officinalis* against third and fourth generation EGFR: Druglikeness, *in silico* ADMET, docking, DFT, molecular dynamics simulation, and MMGBSA study, *Nat. Prod. Res.*, 39 (10), 2970–2977.

[33] Xochicale-Santana, L., Vidyasagar, C.C., Muñoz-Flores, B.M., and Pérez, V.M.J., 2021, Microwave assisted organic syntheses (MAOS): The green synthetic method, *Handb. Greener Synth. Nanomater. Compd.*, 1, 491–542.

[34] Shinde, S.S., Sarkate, A.P., Rathod, S.S., Kilbile, J.T., Chaudhari, S.Y., Yadala, R., Pawar, S.C., and Wakte, P.S., 2024, Synthesis, biological evaluation, and computational studies of thiazolyl hydrazone derivatives as triple mutant allosteric EGFR inhibitors, *J. Chin. Chem. Soc.*, 71 (7), 706–720.

[35] Pawar, C.D., Chavan, S.L., Pawar, U.D., Pansare, D.N., Deshmukh, S.V., and Shinde, D.B., 2019, Synthesis, anti-proliferative activity, SAR, and kinase inhibition studies of thiazol-2-yl-substituted sulfonamide derivatives, *J. Chin. Chem. Soc.*, 66 (3), 257–264.

[36] Karnik, K.S., Sarkate, A.P., Lokwani, D.K., Tiwari, S.V., Azad, R., and Wakte, P.S., 2023, Molecular dynamic simulations based discovery and development of thiazolidin-4-one derivatives as EGFR inhibitors targeting resistance in non-small cell lung cancer (NSCLC), *J. Biomol. Struct. Dyn.*, 41 (10), 4696–4710.

[37] Shinde, S.S., Padule, K.B., Sawant, S.L., and Sarkate, A.P., 2024, "Systems Approach for Identifying Drug Targets by Computational Approaches" in *Systems Biology Approaches: Prevention, Diagnosis, and Understanding Mechanisms of Complex Diseases*, Eds. Joshi, S., Ray, R.R., Nag, M., and Lahiri, D., Springer Nature Singapore, Singapore, 257–270.

[38] Shinde, S.S., Giram, P.S., Wakte, P.S., and Bhusari, S.S., 2025, ADMET tools in the digital era: Applications and limitations, *Adv. Pharmacol.*, 103, 65–80.

[39] Tivari, S.R., Kokate, S.V., Belmonte-Vázquez, J.L., Pawar, T.J., Patel, H., Ahmad, I., Gayke, M.S., Bhosale, R.S., Jain, V.D., Muteeb, G., Delgado-Alvarado, E., and Jadeja, Y., 2023, Synthesis and evaluation of biological activities for a novel 1,2,3,4-tetrahydroisoquinoline conjugate with dipeptide derivatives: Insights from molecular docking and molecular dynamics simulations, *ACS Omega*, 8 (51), 48843–48854.

[40] Shinde, S.S., Bhusari, S.S., and Wakte, P.S., 2024, Exploring the potent anticancer activity of novel phytoconstituent derived from *Zanthoxylum nitidum* using an *in-silico* approach, *Curr. Pharmacogenomics Pers. Med.*, 22, 104–115.

[41] Abdalla, M., Eltayb, W.A., El-Arabey, A.A., Singh, K., and Jiang, X., 2022, Molecular dynamic study of SARS-CoV-2 with various S protein mutations and their effect on thermodynamic properties, *Comput. Biol. Med.*, 141, 105025.

[42] Siva Kumar, B., Anuragh, S., Kammala, A.K., and Ilango, K., 2022, Computer aided drug design approach to screen phytoconstituents of *Adhatoda vasica* as potential inhibitors of SARS-CoV-2 main protease enzyme, *Life*, 12 (2), 315.

[43] Prakash, P., Gayathiri, E., Rahaman, M., Periyasami, G., Pandiaraj, S., Pratheep, T., Selvam, K., Chaudhari, S.Y., Thirumalaivasan, N., Thomas, J., Hatami, M., Govindasamy, R., and Thiruvengadam, M., 2023, Exploring the potential of targeting insulin-like growth factor-1 through network pharmacology, molecular docking, molecular dynamics, and experimental validation of antioxidant and anti-inflammatory activities, *S. Afr. J. Bot.*, 162, 707–718.

[44] Bhandari, S.V., Kuthe, P.V., Patil, S.M., Nagras, O.G., Sarkate, A.P., Chaudhari, S.Y., and Surve, S.V., 2023, Molecular docking, pharmacokinetic and molecular simulation analysis of novel mono-carbonyl curcumin analogs as L858R/T790M/C797S

mutant EGFR inhibitors, *Chem. Biodivers.*, 20 (11), e202301081.

[45] Mohankumar, T., Chandramohan, V., Laliithamba, H.S., Jayaraj, R.L., Kumaradhas, P., Sivanandam, M., Hunday, G., Vijayakumar, R., Balakrishnan, R., Manimaran, D., and Elangovan, N., 2020, Design and molecular dynamic investigations of 7,8-dihydroxyflavone derivatives as potential neuroprotective agents against alpha-synuclein, *Sci. Rep.*, 10 (1), 599.

[46] Gaikwad, N.M., Chaudhari, P.D., Shaikh, K.S., Chaudhari, S.Y., Saleem, R.M., Algahtani, M., Altyar, A.E., Albadrani, G.M., Kamel, M., and Abdel-Daim, M.M., 2023, Albendazole repurposing on VEGFR-2 for possible anticancer application: *In-silico* analysis, *PLoS One*, 18 (8), e0287198.

[47] Zaki, M.E.A., Al-Hussain, S.A., Al-Mutairi, A.A., Samad, A., Ghosh, A., Chaudhari, S., Khatale, P.N., Jawarkar, R.D., and Jawarkar, R.D., 2023, *In-silico* studies to recognize repurposing therapeutics toward arginase-I inhibitors as potential onco-immunomodulators, *Front. Pharmacol.*, 14, 1129997.

[48] Lee, Y., Lee, S., Lee, Y., Song, D., Park, S.H., Kim, J., Namkung, W., and Kim, I., 2024, Anticancer evaluation of novel benzofuran–indole hybrids as epidermal growth factor receptor inhibitors against non-small-cell lung cancer cells, *Pharmaceuticals*, 17 (2), 231.

[49] Mirgany, T.O., Motiur Rahman, A.F.M., and Alanazi, M.M., 2024, Design, synthesis, and mechanistic evaluation of novel benzimidazole-hydrazone compounds as dual inhibitors of EGFR and HER2: Promising candidates for anticancer therapy, *J. Mol. Struct.*, 1309, 138177.

[50] Yamauchi, M., Kitamura, Y., Nagano, H., Kawatsu, J., and Gotoh, H., 2024, DPPH measurements and structure–activity relationship studies on the antioxidant capacity of phenols, *Antioxidants*, 13 (3), 309.

[51] Jaber, Q.A.H., Shentaif, A.H., Almajidi, M., Ahmad, I., Patel, H., Azad, A.K., Alnasser, S.M., Alatawi, H.A., Menaa, F., Alfaifi, S.Y., Rahman, M.M., Ali, M.M., and Rao, S.J.A., 2023, Synthesis, structure, and *in vitro* pharmacological evaluation of some new pyrimidine-2-sulfonamide derivatives and their molecular docking studies on human estrogen receptor alpha and CDK2/cyclin proteins, *Russ. J. Bioorg. Chem.*, 49 (1), S106–S118.